Annals of Nuclear Energy 134 (2019) 125–133

Contents lists available at ScienceDirect

Annals of Nuclear Energy

journal homepage: www.elsevier.com/locate/anucene

The transport and decay of radioactive aerosols in a wall-bounded turbulent flow

Weiguo Gu, Jinpeng He, Dezhong Wang *, Yuxiang He

School of Mechanical Engineering, Shanghai Jiao Tong University, Shanghai 200240, China

A R T I C L E I N F O

Article history:
Received 24 February 2019
Received in revised form 3 May 2019
Accepted 13 May 2019

Keywords:
Radioactive aerosol
Radioactivity
Lagrangian particle tracking
Radioactive decay
Particle deposition
Wall-bounded turbulent flow

A B S T R A C T

This paper aims at radiation monitoring and activity inversion when radionuclides are transported in duct or a pipe. The Lagrangian trajectory model was established, and a quick numerical method was used to simulate radioactive aerosols transport and radioactive decay in a wall-bounded flow. Total 12 cases were studied in the simulation according to the particle diameter and density. The dimensionless deposition velocity has been validated by comparing with Wood's predictions and the experienced gravitational settling velocity. The results show that turbophoresis has a significant effect on particle transport in the wall-bounded flow, leading to particles migration and concentrating near the wall or channel center. It will cause particles to move with different velocities in the streamwise direction, so that their residence times in channel will be complexly distributed. In addition, the gravity settling will enhance the disequilibrium of particle distribution. The activity losses are obtained in detail including particle deposition ratio and radioactive decay. One radionuclide with half-life 7 s was employed in simulation, and the activity error between the estimated and initial values is up to about 40%. The activity error decreases if the half-life becomes large. When the half-life is 7.5 and 0.5 times larger than the mean time spent by airflow through the channel if the gravity is considered or not respectively, the final activity error will be less than ±5% in the present simulation setup.

1. Introduction

The regulatory guide 1.45 published by U.S. Nuclear Regulatory Commission mentions that it is very important to continuously monitor and quantify the reactor coolant leakage for ensuring the safe operation of the facility (Regulatory guide 1.45, 2008). One of the efficient methods to consider for incorporation in the technical specifications is to monitor airborne particulate radioactivity. Some short half-lived nuclides are considered such as ^{19}O, ^{16}N, ^{13}N, ^{18}F and ^{3}H. During the monitoring, airborne particles are sampled and pumped in pipe lines. According to the requirements by the International Organization for Standardization (ISO), a representative sample is necessary in monitoring the activity concentrations of radioactive substances (ISO, 2889). The losses of aerosol particles in the transport lines due to particle deposition therefore needs to be determined.

The depositions during particle transport in a turbulent flow include gravitational settling and sedimentations on the walls caused by Brownian diffusion, turbophoresis, thermophoresis and other factors. The fundamental phenomenon of small aerosols drifting down a temperature or turbulence gradient is called thermophoresis or turbophoresis. The turbophoretic effect has been widely studied that inertial particles migrates in the direction of decreasing turbulence level and accumulate in minima of turbulence intensity (Brooke et al., 1992; Sardina et al., 2012). Some experiments also shows that particles in a turbulent pipe flow are not distributed uniformly at the exit of the pipe while they concentrates near the pipe axis or the wall depending on particles' Stokes number (Lau and Nathan, 2014). Coherent flow structures especially in the boundary layer is considered to cause the remarkably accumulation of macroscopic particles in the viscous sublayer (Narayanan and Lakehal, 2003; Marchioli et al., 2003). The deposition of particles near the wall is related with some dimensionless parameters such as relaxation time and Stokes number. The particles with relatively lower Stokes number will move preferentially toward the wall, which was found by particle-resolved direct numerical simulations (Jebakumar et al., 2019). According to the characterization of particle deposition velocity versus non-dimensional relaxation time, three distinct regimes were identified, such as the diffusive deposition regime, the turbulent diffusion-eddy impaction regime and the particle inertia moderated regime (Chiou et al., 2011).

* Corresponding author.
E-mail address: dzwang_sjtu@sina.com (D. Wang).

https://doi.org/10.1016/j.anucene.2019.05.023
0306-4549/

The long-term accumulation will lead to the non-uniform spatial distribution of particles as well as the complex distribution of residence times and decay for radioactive nuclides contained in the particles. It was found that radioactive aerosols are inherently multicomponent due to radioactive decay (Kim et al., 2017). One study has been carried out for monitoring fission products with halftime varying from 76.3 min (^{87}Kr) to 30 years (^{137}Cs) released into atmosphere by a combined model of radionuclides transport/decay/coagulation (Aloyan et al., 2000). For the long distance transport of radionuclides in the atmosphere, the power-law relationship was used to determine the minimum magnitude of sampler activity according to the distance from the source (Eslinger et al., 2015). The decay correction was proposed by using sampling time in determination of activity concentration of short-lived radionuclides based on the function of the exponential decrease of the delay time (Jiménez-Ramos et al., 2006).

However, the decay correction is not mentioned when nuclides are transported in pipe lines for monitoring airborne particulate radioactivity in ISO-2889. Although the decay can be ignored for long-lived radionuclides, it can have a large effect on the short-lived radionuclides. The turbophoresis results in particle concentration near the axis or the wall, but the influence of turbophoresis on the radioactive decay correction has not been studied. This paper focuses on the turbophoresis effect on particles migration and residence times in the channel. The characteristics of radioactive decay was studied and the final monitoring activity errors were compared with the estimates based on the negative exponential function of the half-life and mean fluid time.

2. Methodology

Aerosol particles are spread and tracked in the air fluid where the channel is shown in Fig. 1. In order to study the influence of wall-bounded fluids on the particles transport and deposition in one dimension, infinite walls were applied in the computational domain. Therefore, a periodic boundary was set in the spanwise (z) direction. The horizontal and vertical walls in the duct were simulated depending on whether the gravity was set in the wall-normal (y) direction or not. The geometrical dimensions of the computational domain in streamwise (x), wall-normal (y), spanwise (z) directions were 25 m, 100 mm and 200 mm respectively.

The particles spread in the channel were assumed to be spherical. Because the particles volume concentration is far less than $10^{12}\ \mathrm{m}^{-3}$, the collision and coalescence between particles were neglected (Li et al., 2018). The gravity (F_G), buoyancy (F_b), air drag force (F_D), and Brownian force (F_B) were considered to act on particles. According to the activity concentration of fissionable and activated nuclides in the primary loop of nuclear power plant, the activity of the nuclides dispersed in one particle would be too low to obtain a significant self-charging, so the charge was ignored in this situation if there was no electrical field (Gensdarmes et al., 2000). The virtual mass force and the Basset force were also not included because they are small when the ratio of particle density and fluid density are large and Reynolds number is comparatively small (Guha, 2008). The forces considered in this simulation are expressed by (Li et al., 2018)

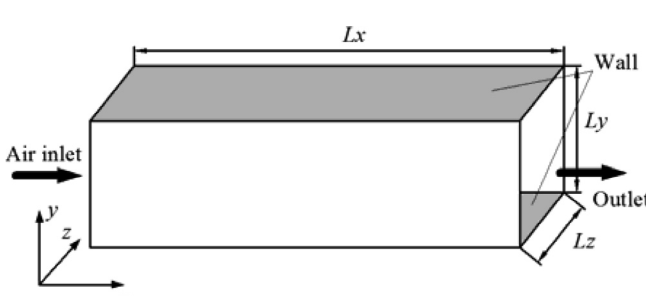

Fig. 1. Computational domain of the wall-bounded turbulent flow.

$$F_G = \frac{1}{6}\pi\rho_p d_p^3 g \tag{1}$$

$$F_b = \frac{1}{6}\pi\rho_a d_p^3 g \tag{2}$$

$$F_B = R(0,1)\cdot\sqrt{\frac{\pi S_0}{\Delta t}} \tag{3}$$

$$F_D = \frac{1}{8}\pi d_p^2 C_D \rho_a |V_a - V_p|(V_a - V_p) \tag{4}$$

where ρ_a and ρ_p (kg/m^3) are the densities of air and particle; V_a and V_p (m/s) are the velocities of airflow and particle; d_p (m) is the aerodynamic diameter of particles; g (m/s^2) is the gravity acceleration. R (0,1) is a random number generated by the standard Gaussian function; Δt (s) is a time spacing. S_0 is the spectral intensity function estimated by

$$S_0 = \frac{216\upsilon_a k_B T}{\pi^2\rho_a d_p^5\left(\rho_p/\rho_a\right)^2 C_u} \tag{5}$$

where T (K) and υ_a (m^2/s) is the absolute temperature and kinematic viscosity of the air, respectively; k_B is the Boltzmann constant; C_u is the Stokes-Cunningham slip correction factor. C_D is the drag coefficient which is a function of the particle Reynolds number $Re_p = d_p|V_a - V_p|/\upsilon_a$. Due to the particle Reynolds number less than one in this simulation condition, C_D can be calculated by $C_D = 24/Re_p$. The kinetic equation of particle movement is established by

$$F_{D,i} + F_i = m_p\frac{\mathrm{d}V_{p,i}}{\mathrm{d}t} \tag{6}$$

where i = 1, 2, 3 represent the x, y, z direction respectively; m_p (kg) is the particle mass. F_i includes all forces needed in i direction except the drag force. If the drag force is applied to Eq. (6), the kinetic equation is simplified to

$$3\pi d_p\mu_a(V_a - V_p)_i + F_i = m_p\frac{\mathrm{d}V_{p,i}}{\mathrm{d}t} \tag{7}$$

where $\mu_a = \upsilon_a\cdot\rho_a$ is the dynamic viscosity of airflow. Due to the very small of the time step, it is assumed that F and V_a are not changed within one time step, the particle velocity in the (n + 1)th time step can be obtained by the integral of Eq. (7).

$$\int_t^{t+\Delta t}\frac{3\pi d_p\mu_a}{m_p}\mathrm{d}t = \int_{V_p^n}^{V_p^{n+1}}\frac{3\pi d_p\mu_a}{3\pi d_p\mu_a(V_a - V_p) + F}\mathrm{d}V_p \tag{8}$$

The particle velocity and position in the (n + 1)th time step are as follows.

$$V_{p,i}^{n+1} = \left(V_{a,i}^n + \frac{F_i}{3\pi d_p\mu_a}\right)\left(1 - e^{-\frac{3\pi d_p\mu_a}{m_p}\Delta t}\right) + V_{p,i}^n e^{-\frac{3\pi d_p\mu_a}{m_p}\Delta t} \tag{9}$$

$$x_{p,i}^{n+1} = x_{p,i}^n + 0.5\left(V_{p,i}^n + V_{p,i}^{n+1}\right)\cdot\Delta t \tag{10}$$

During calculating particle movements, the local air velocities in each time step were generated according to the particle positions. A stochastic method introduced by the reference (Gu et al., 2019) was adopted in this simulation. This method proposes that the mean streamwise velocity of airflow is obtained by the interpolation in the statistical curves, velocity fluctuations are generated

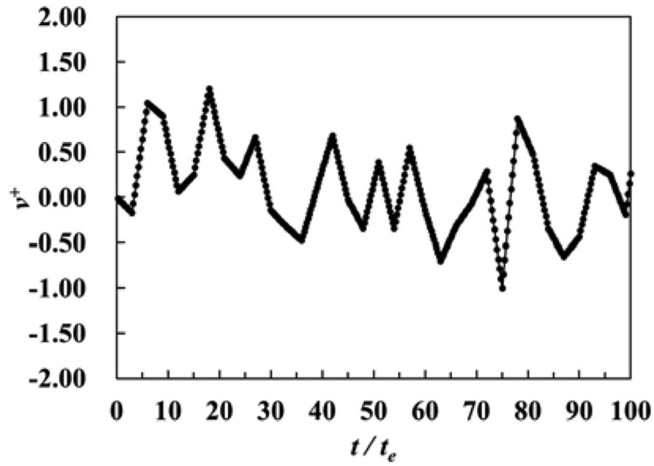

Fig. 2. The sampling wall-normal velocities generated by the stochastic method at $y^+ = 100$.

by random data based on root mean square (σ) of velocity fluctuations ($\upsilon_a = V_a - \overline{V_a}$), and Reynolds shear stress are obtained by the direct numerical simulation (DNS) or experiments.

Since the simulation is sensitive to the time step, the Δt which was 0.25 and 0.5 times of t_e was employed in the simulation (Gu et al., 2019; Mito and Hanratty, 2002), where $t_e = \upsilon_a / u^{*2}$ is the average lifetime of the smallest eddy in near-wall regions, u^* is the friction velocity of airflow in the channel. However, Mito and Wang found that the Eulerian time scales for a turbulent flow in a channel are about three times of t_e when dimensionless Reynolds number is 150 (Mito and Hanratty, 2002; Wang et al., 2011). The time scale are much larger than the time spacing employed in the simulation. Considering the velocity fluctuations are changed gradually within the time scale, the velocity fluctuations were generated by the stochastic method per time scale which is equal to $3t_e$ and linearly interpolated per time step in the simulation. The time scale was divided equally into 12 parts, so the time spacing is $\Delta t = 0.25t_e$. Fig. 2 shows the sampling velocity of airflow versus the time in the position at $y^+ = 100$ where $y^+ = u^* \cdot y / \nu_a$. It can ensure that the time spacing in this simulation is small and coincides with the setup by Mito, while time scale of turbulence is similar with the statistical characteristics in DNS.

3. Results and discussion

The discussion includes two situations when the gravity is not considered and considered in the -*y* direction. The gravitational settling will not appear in the former situation. The temperature and pressure of airflow are 293 K and 1 atm, respectively. The dimensionless Reynolds number $Re_\tau = u^* L_y / 2\upsilon_a$ is 150. Table 1 shows the totally 12 cases in simulation including three diameters of 0.1, 1.0, 10.0 μm and two densities of 1.0, 2.5 g/cm^3.

3.1. The verification of deposition velocity

The initial particles are set to be uniformly distributed in the channel. If the particle touches the wall, it is assumed to stick on the wall and deposit. The dimensionless deposition velocity is estimated by

$$V_d^+ = \frac{N_d}{N} \cdot \frac{L_y}{\Delta t_d \cdot u^*} \tag{11}$$

where N is the initial number of particles distributed in the channel; N_d is the number of particles depositing on a wall within a certain time intervals Δt_d. Wood (Wood, 1981) once proposed a semi-empirical correlation between the dimensionless deposition velocity (V_d^+) and dimensionless particle relaxation time (τ^+) when gravitational settling was excluded.

$$V_d^+ = 0.057 Sc^{-2/3} + 4.5 \times 10^{-4} \tau^{+2} \tag{12}$$

If gravitational settling was included, the dimensionless gravitational settling velocity V_g^+ should be added into Eq. (12). V_g^+ is defined as

$$V_g^+ = \tau^+ g^+ = \tau^+ \cdot \frac{\upsilon_a}{u^{*3}} g \tag{13}$$

where $\tau^+ = \tau \cdot u^{*2} / \upsilon_a$ is the dimensionless particle relaxation time and $\tau = \rho_p d_p^2 C_u / 18\mu_a$; $Sc = \upsilon_a / D$ is the Schmidt number; D is the molecular diffusivity.

The cases numbered 1–6 in Table 1 exclude the gravitational settling. In the table, τ^+ ranges from 1.41×10^{-5} to 0.115, V_d^+ decreases with the increase of τ^+ due to the weakened Brownian diffusion. The cases numbered 7–12 include the gravitational settling. V_g^+ rapidly increases to be in charge of the total deposition velocity when the particle diameter and density become larger. The relative error of dimensionless deposition velocity ($V_{d,s}^+$) to Wood's predictions ($V_{d,w}^+$) is defined as $\delta_{vd} = \left(V_{d,s}^+ - V_{d,w}^+\right) / V_{d,w}^+ \times 100\%$. It can be seen that the deposition velocities obtained by the simulation agree well with the Wood's predictions for all cases with the absolute relative errors less than 15%.

3.2. The transport and deposition of particles

First the gravity is not included in order to discuss the influence of turbulence on particle transport. The particles are uniformly released in the channel inlet and tracked individually. 40 particle

Table 1
The simulation cases and dimensionless deposition velocity.

	Case	Diameter μm	Density kg/m^3	τ^+	V_g^+	$V_{d,w}^+$	$V_{d,s}^+$	δ_{vd}
1	No gravity	0.1	1000	1.41E-05	0	7.64E-05	8.76E-05	14.66%
2		1.0	1000	5.34E-04	0	8.61E-06	7.96E-06	−7.59%
3		10.0	1000	4.59E-02	0	2.63E-06	2.54E-06	−3.29%
4		0.1	2500	3.53E-05	0	7.64E-05	8.06E-05	5.53%
5		1.0	2500	1.34E-03	0	8.61E-06	9.09E-06	5.52%
6		10.0	2500	1.15E-01	0	7.61E-06	7.88E-06	3.57%
7	Gravity in the -*y* direction	0.1	1000	1.41E-05	1.99E-05	9.63E-05	8.96E-05	−6.95%
8		1.0	1000	5.34E-04	7.54E-04	7.63E-04	7.19E-04	−5.76%
9		10. 0	1000	4.59E-02	6.48E-02	6.48E-02	7.38E-02	13.83%
10		0.1	2500	3.53E-05	4.98E-05	1.26E-04	1.29E-04	2.25%
11		1.0	2500	1.34E-03	1.89E-03	1.89E-03	2.16E-03	14.02%
12		10.0	2500	1.15E-01	1.62E-01	1.62E-01	1.63E-01	0.57%

trajectories in case 2 are shown in Fig. 3(a). The trajectories are rugged when particles are transported by the combined effect of turbulent fluctuations and Brownian diffusion. The relative coordinates are $x_i^* = x_i/(L_y/2)$. Fig. 3(b) shows the rest particles distributed in the outlet after the deposition on the wall. It can be observed that the distribution is not uniform. The particles are concentrated in two areas, the central area with $0.6 < y^* < 1.4$ and areas near the wall which is similar with the findings by Lau (Lau and Nathan, 2014).

The particle number in the outlet is statistically counted in 30 equispaced bins along the wall-normal direction where the area is at $0 < y^+ < 150$ and the spacing is $\Delta y^+ = 5$. The relative number in the j-th bin is defined as

$$C_j^* = N_{y^+\in(j\times 5, j\times 5+5)}/N_0 \tag{14}$$

where N_0 is the initial number of particles released in the inlet; $j = 0, 1, \ldots, 29$ is the serial number of each bin. Fig. 4 shows the distributions of C^* in each bin whose y-coordinate is set as $y_j^+ = (j + 0.5)\Delta y^+$. It can be seen that the distribution curves of the first six cases are overlap and appear "U" pattern.

The relative number is comparatively small where y^+ is larger than 10 and less than 50, which further proves the particle accumulation in the areas near the channel center and the wall.

The particle accumulation is related with the turbulence characteristics. The root mean square (*rms*) of air wall-normal velocity fluctuation σ_y is defined as $\sigma_y = \sqrt{\sum V_a^2/N}$, where V_a is air wall-normal velocities whose mean value is equal to zero; N is the number of velocities used in statistical calculation. As shown in Fig. 5, σ_y increases sharply from zero to the top ($y^+ = 60$), then decreases gradually with the increases of y^+. The large value of σ_y indicates the high turbulence which results in fast moving and quick fleeing of particles, so that particles leaving the region will be more than those entering the region. This process is called turbophoresis and influences the particle trajectories and the deposition.

In addition, Fig. 4 also shows the overlap curves of C^* distribution versus y^+. In order to study the dependence of particles diameter and density on following characteristics in the airflow, the relative root mean square of wall-normal velocity difference between particles ($V_{y,p}$) and airflow ($V_{y,a}$) is defined as follows.

$$\varepsilon_y^* = \sqrt{\sum (V_{y,p} - V_{y,a})^2/N}/\sigma_y \tag{15}$$

As shown in Fig. 6, ε_y^* is less than 1% of σ_y when $y^+ > 10$, which indicates that particles in these cases follow well the airflow and C^* is distributed similarly with each other. Due to the Brownian motions, ε_y^* is a little larger for smaller diameter particles than those with larger diameter. In case 6 when the particle diameter is 10 μm and density is 2.5 g/cm^3, ε_y^* has the largest value in the

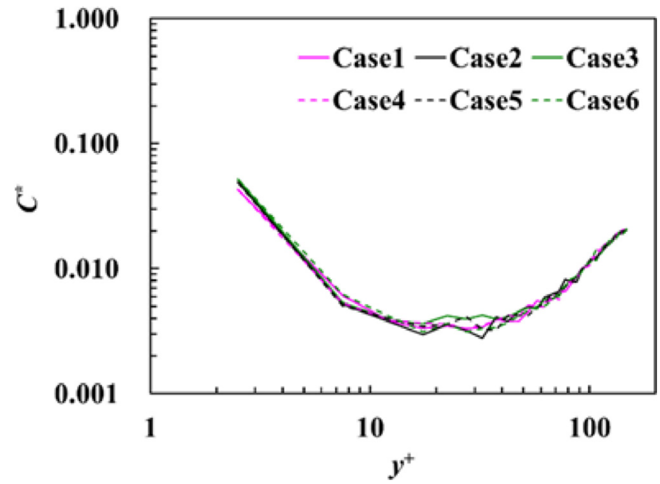

Fig. 4. The relative number of particles in the outlet distributed along wall-normal direction for the first six cases.

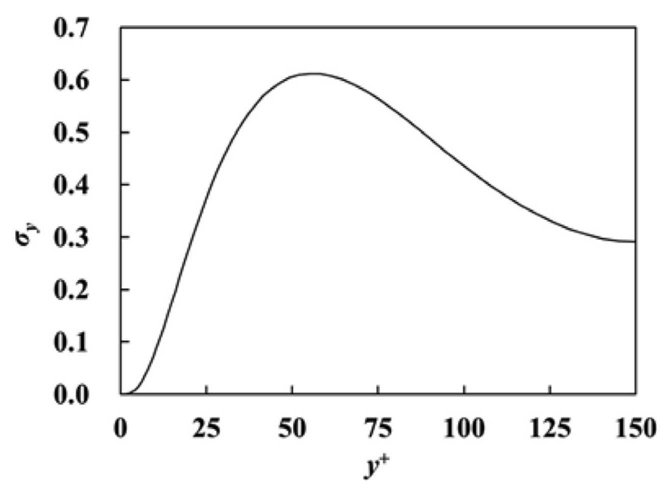

Fig. 5. The *rms* of air wall-normal velocities distributed along wall-normal direction.

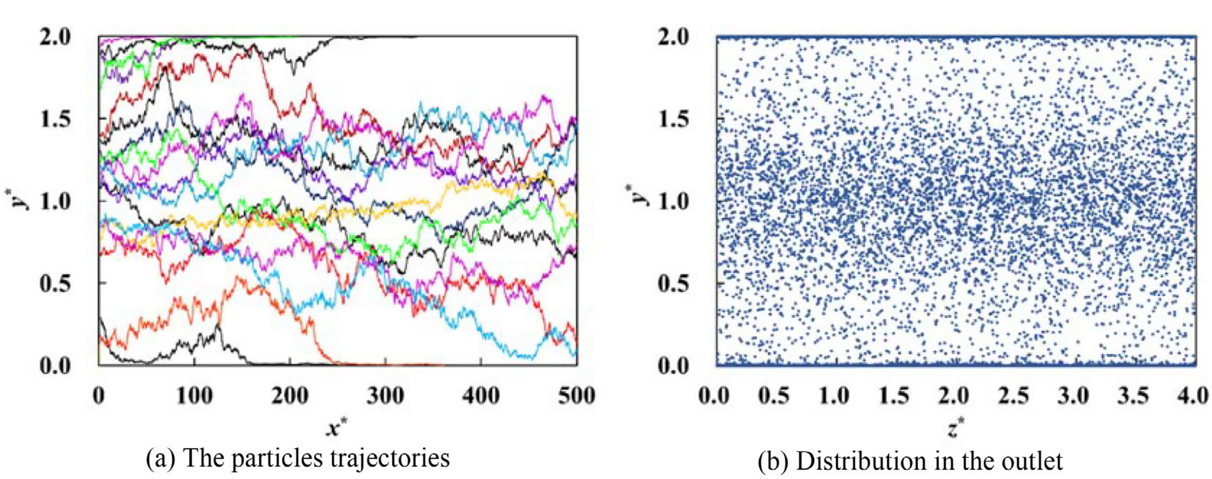

Fig. 3. Particles trajectories and distribution in the outlet when the diameter and density are 1 μm and 1 g/cm^3.

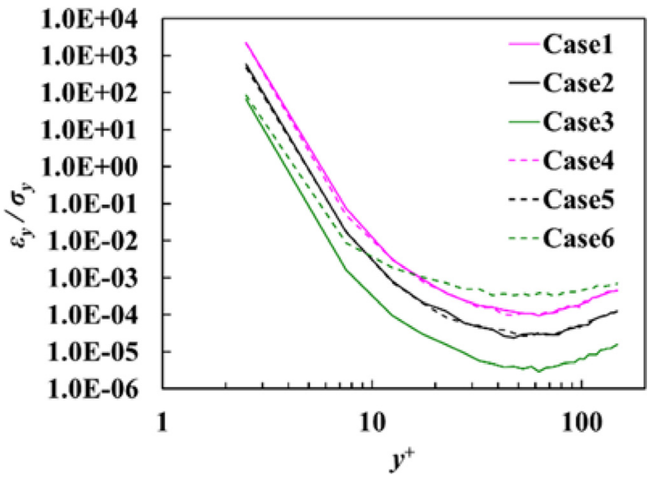

Fig. 6. The relative *rms* of wall-normal velocity differences distributed along wall-normal direction.

area of $y^+ > 20$ because the large inertia delays the response to turbulence fluctuations. At the same time, when particles are at $y^+ < 10$, Brownian diffusion is gradually in charge of this region, leading to gradual increase of ε_y^*.

Although the relative number is distributed similarly for the first 6 cases, the deposition velocities are different. When y^+ is less than 10, the particle relative number at different time $t^+ = t/t_e$ is shown in Fig. 7. The relative deposition number $\zeta = N_d/N_0$ is the ratio of total depositing number before t^+ on the wall at $y^+ = 0$ to the initial number. It can be found that the relative number initiates from the original concentration, starts to increase at about $t^+ = 30$, reaches the top at $t^+ = 7000$, then decreases because of the increasing deposition. The deposition starts at about $t^+ = 4000$, sharply increases from the time about $t^+ = 10000$. It is concluded that particles will move slowly or stop in the viscous layer and then deposit gradually, which coincides with the findings of particle accumulation in the viscous layer y (Narayanan and Lakehal, 2003). Fig. 7(b) shows the particles with diameter of 0.1 μm deposit more obviously than other cases, which indicates the stronger effects of Brownian diffusion on smaller particles. When the diameter and density become larger, the larger inertia will delay the response of Brownian diffusion, the deposition number and deposition velocity accordingly are reduced. As a result, those particles with diameters less than 10 μm can follow the airflow well outside the viscous layer, but the deposition process will be not influenced by turbulence but Brownian diffusion inside the viscous layer when the gravitational settling is not considered.

When the gravity is set in the $-y$ direction, the particle deposition will lead to the reduction of particle concentration. As shown in Fig. 8, the particles with diameter of 10 μm have almost entirely deposited in the bottom wall. Particularly, the particles of case 12 have disappeared in the outlet. For the particles whose diameters are 0.1 and 1 μm, the number concentrations are similarly distributed in the areas at $y^+ > 10$, but the 1 μm particles are fewer than 0.1 μm particles if $y^+ < 10$. It can be concluded that the turbulence in the main flow region is strong enough to be in charge of the transport of micron and submicron particles even though the gravity acts on the particles. When the turbulence is weakened inside the viscous layer, the gravity will drive the micron particles to deposit faster than submicron particles.

Fig. 9 shows the relative number of particles in the areas at $y^+ < 10$ at different time when the gravitational settling is considered in the wall-normal direction. The10 μm particles deposit quickly in the viscous layer, especially when the density is 2.5 g/cm^3. The particles start to deposit at about $t^+ = 30$, and all have deposited before $t^+ = 3000$. When the density is 1 g/cm^3, about 95% particles have deposited before $t^+ = 6000$. At the same time, the 0.1 μm particles will be accumulated in the viscous layer

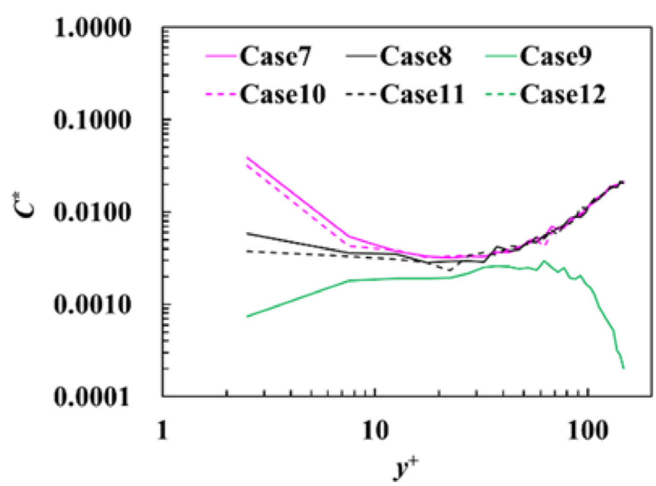

Fig. 8. The relative number of particles in the outlet distributed along wall-normal direction when gravitational settling is considered.

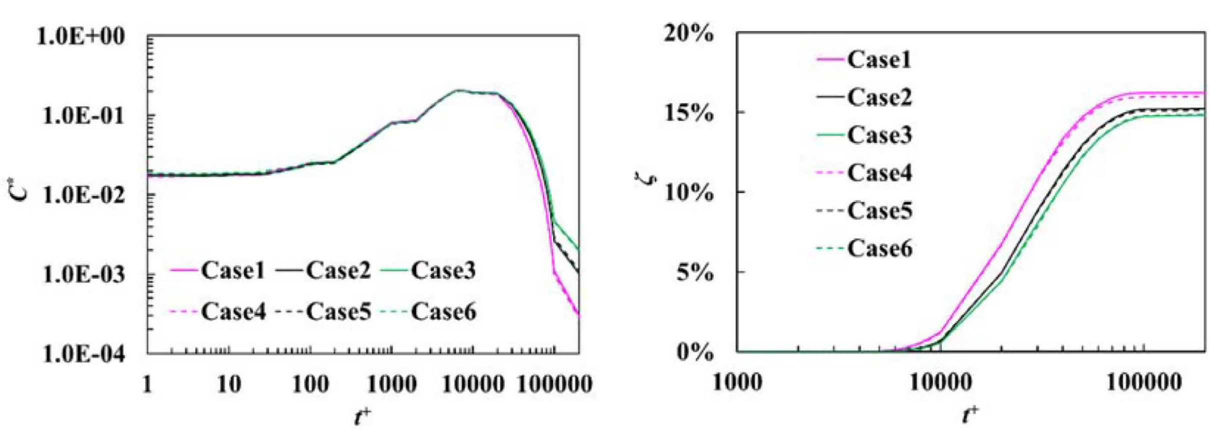

(a) C^* in the areas at $y^+<10$

(b) The relative number of depositions

Fig. 7. The relative number of particles at $y^+ < 10$ and depositions at different time when gravitational settling is not considered.

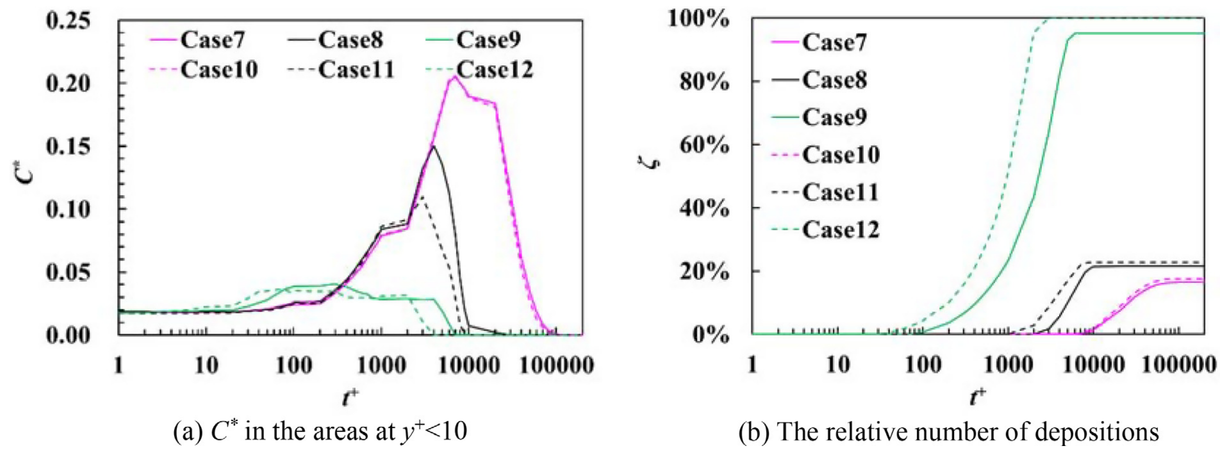

Fig. 9. The relative number of particles at $y^+ < 10$ and depositions at different time when gravitational settling is considered.

first, the number concentration reaches the top at $t^+ = 8000$, finally about 17% particles have deposited. The 1 μm particles start to deposit at about $t^+ = 2000$, and about 23% particles have deposited finally. On the whole, particles with larger density will start to deposit earlier. All particles in the viscous layer can deposit on the bottom wall. The micron and submicron particles are mainly distributed in the main flow region.

3.3. Radioactive decay of radioactive aerosols

In addition to the deposition, radioactive decay will affect the final relationship between initial activity and statistical activity in the outlet. The final activity and its distribution depend on the half-life of radionuclides and the residence times of particles along their trajectories in the channel. There are a lot of short half-lived nuclides produced by the fission or activation, such as I-113m, N-16, Ba-137m, N-13, Rh-106, O-19, Rb-88, Te-131 and so on. This paper will not focus on one detailed nuclide. Two half-lives of 7 s and 600 s are adopted for the comparison. In the simulation, one type of nuclide is assumed to be contained uniformly within the aerosol particles.

The total activity in the outlet can be counted based on that containing in each particle. If N particles have passed through the outlet, the total activity is

$$\sum_{1\le n\le N} A_n = \sum_{1\le n\le N} A_0 e^{-\ln 2\cdot t_n/t_{1/2}} \tag{16}$$

where $t_{1/2}$ (s) is the half-life; t_n (s) is the residence time of the n-th particle; A_0 (Bq) is the initial activity in a particle. The total activity in the inlet is N_0A_0. The total activity in the outlet relative to the initial total activity is

$$\frac{\sum_{1\le n\le N} A_n}{N_0A_0} = \frac{N\cdot\bar{A}}{N_0A_0} = (1-\zeta)\cdot\frac{1}{N}\sum_{1\le n\le N} e^{-\ln 2\cdot t_n/t_{1/2}} \tag{17}$$

where ζ is the relative number of particles depositing in both walls; $\bar{A}$ is the mean activity inside one particle in the outlet.

$$\frac{\bar{A}}{A_0} = \frac{1}{N}\sum_{1\le n\le N} e^{-\ln 2\cdot t_n/t_{1/2}} \tag{18}$$

Therefore, the total activity in the outlet can be estimated by Eq. (17) and depends on the number of deposition and the residence time for each particle through the channel. In the practical situation, it is difficult to obtain the detailed residence time for each particle, the mean time of airflow ($\overline{t_{air}}$) usually is used in the activity calculation.

$$\overline{t_{air}} = L_x/\overline{U_{air}} \tag{19}$$

In the above equation, $\overline{U_{air}}$ (m/s) is the mean air streamwise velocity; L_x (m) is the channel length. The mean activity in a particle in the outlet ($\overline{A_e}$) is calculated by follows.

$$\overline{A_e} = A_0 e^{-\ln 2\cdot \overline{t_{air}}/t_{1/2}} \tag{20}$$

Due to the effect of turbophoresis, particle trajectories and residence times are different individually. Fig. 10 exhibits the residence times of all particles through the outlet distributed versus their y coordinates when the gravidity is not set. It is observed that the residence times are very close to the airflow time in the area at $y^+ > 10$, but they are dispersed where y^+ is less than 10. In the figure, the time estimated by air denotes the local airflow time $t_{air} = L_x/U_{air,y}$ at a fixed y-coordinate. The time estimated by airflow is much larger than residence times of most particles at $y^+ < 10$. It is known that turbophoresis will drive particles to migrate from the main flow region toward the wall, so a lot of particles are not the native particles in the viscous layer. The mean velocity of a particle along its trajectory is larger than its final velocity, so that the residence time is smaller than the airflow time at the final position of the particle.

The activity distribution in the outlet are also counted in 30 equispaced bins along y direction, and is shown in Fig. 11. In the figures, the activity estimated by air is $A = A_0 e^{-\ln 2\cdot t_{air}/t_{1/2}}$ at a fixed

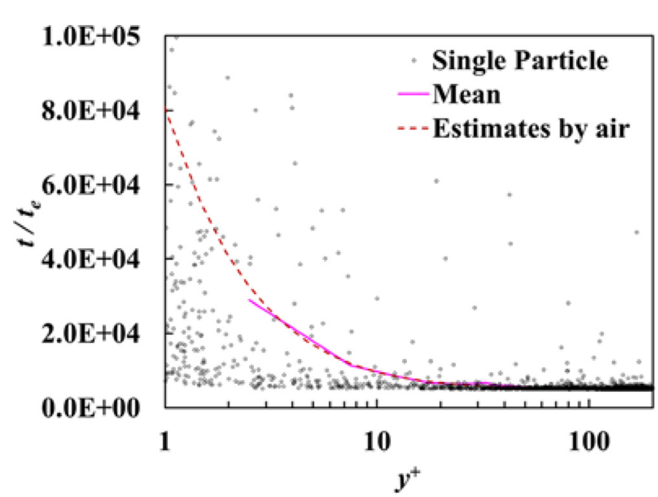

Fig. 10. The distribution of residence times of particles in the outlet whose diameter and density are 1 μm and 1 g/cm^3 when the gravity is not considered.

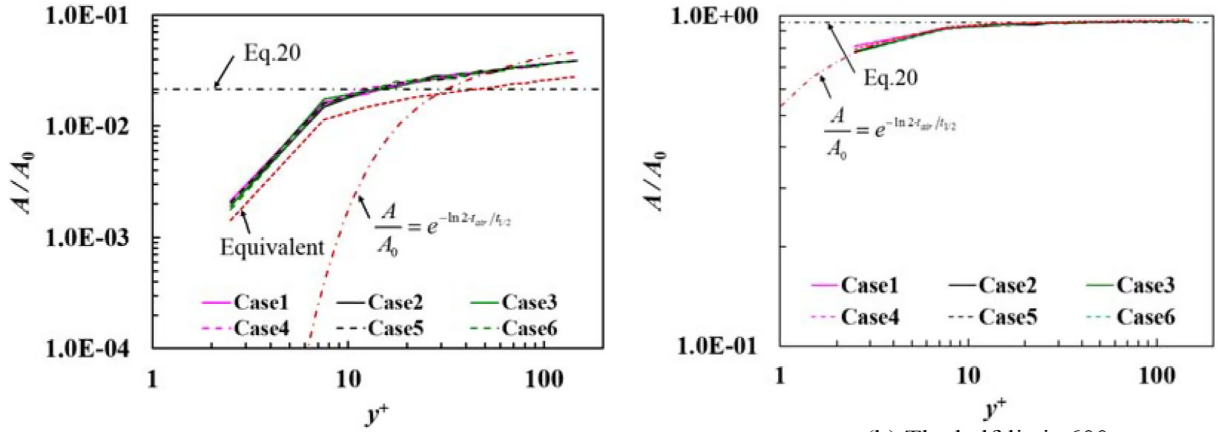

(a) The half-lie is 7 s

(b) The half-lie is 600 s

Fig. 11. The statistical distribution of activities in the outlet along the wall-normal direction when the gravity is not considered.

y-coordinate. As shown in Fig. 11, the activity distributions are quite different with the estimate by air when the half-life is 7 s. It can be seen that the mean activity counted in each bin is several orders of magnitude larger than that estimated by air when $y^+ < 50$, whereas it is a little smaller than the estimated value in the channel central areas. Due to turbophoresis leading to particle concentration in two areas, the mean activity in the area near the wall will be larger than the estimate by air, while it is smaller than the estimate in channel central areas. The comparison between the two parts will determine whether the total activity is larger than the estimate. The activity obtained by Eq. (20) is the mean value of estimate by air at different y-coordinates. The curve labeled "Equivalent" is the hypothetical curve whose mean value equals the activity obtained by Eq. (20). Obviously, the curves of cases numbered 1–6 in Fig. 11(a) move upper than the "Equivalent" curve. It is concluded that the real mean activity in the outlet will be larger than the estimate by air. However, when the half-life becomes 600 s as shown in Fig. 11(b), the radioactive decay is very slight in the present situation, all curves are well overlapped with each other. In this case, the real activity in the outlet is close to the estimate by air.

When the gravity is considered in the wall-normal direction, it will influence particle trajectories especially in the areas near the upper wall. Fig. 12 shows the distribution of particle residence times in the outlet. The x coordinate of the figure is $y^*=2y/L_y$ which ranges from 0 to 2 and covers the whole width of the channel. It is found that the distribution is not symmetrical to the channel central plane. The particles near the bottom wall have deposited. The residence times of the rest particles are smaller than that estimated by air. At the same time, the particles near the upper wall at $y^* = 2$ are settled by gravity and enter the main flow region. Their streamwise velocities are increasing, but the mean value is smaller than the local air velocity where particles arrive, so the residence times are larger than the time estimated by the local air.

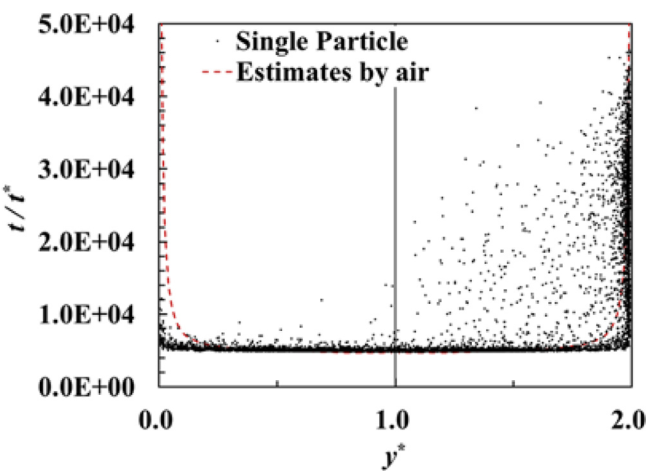

Fig. 12. The distribution of residence times of particles in the outlet whose diameter and density are 1 μm and 1 g/cm^3 when the gravity is considered.

The activity and relative number distributed along y coordinate are shown in Fig. 13 when gravitational settling is considered in the wall-normal direction. In cases 9 and 12 when the diameter is 10 μm, almost all particles have deposited in the bottom wall, so their activities are not discussed. Fig. 13 shows the results for the radionuclide with half-life of 7 s. It is observed that the activities in cases 8 and 11 are a litter larger than that in cases 7 and 10 in the area near the bottom wall because the depositions of large particles are more than that of small particles under the effect of gravity. But in the area at $y^* > 1$, the activities in cases 8 and 11 are obviously smaller than that in cases 7 and 10. Meanwhile, the 0.1 μm particles will still deposit on the upper walls. The particle number in cases 7 and 10 is smaller than that in cases 8 and 11. As a result, the mean activity in cases 7 and 10 is larger than that in cases 8 and 11. In the figure, the curve labeled "Equivalent" is the hypothetical one referenced the distribution in case 8 when the mean value equals the activity obtained by Eq. (20). The hypothetical curve is the lowest in the figure. It shows that the mean activity in the outlet is larger than the estimate by air.

In order to contrast the real mean activity in the outlet with the estimate, the activity error is defined as

$$\Delta_A = \left(\overline{A} - \overline{A_e}\right)/\overline{A_e} \times 100\% \tag{21}$$

where $\overline{A}$ is the real mean activity in the outlet obtained by Eq. (18), $\overline{A_e}$ is the activity estimate obtained by Eq. (20).

Table 2 shows the statistical results including the relative number (ζ) of depositions in the bottom and upper walls, activity errors for the two radionuclides. In cases 1–6, the percentages of particles depositing in both walls are very close and about 15%. The activity errors range from 40% to 45% when the half-life is 7 s, whereas the errors are very small for all 12 cases when the half-life is 600 s. In cases 7–12, particles will deposit in both walls when the diameter is 0.1 μm. The deposition percentage in the bottom wall is lager by 1% and 3% than that in the upper wall when the densities are 1 and 2.5 g/cm^3 respectively. If the diameter is 1 μm, 22% particles will deposit in the bottom wall, but no particle deposits in the upper

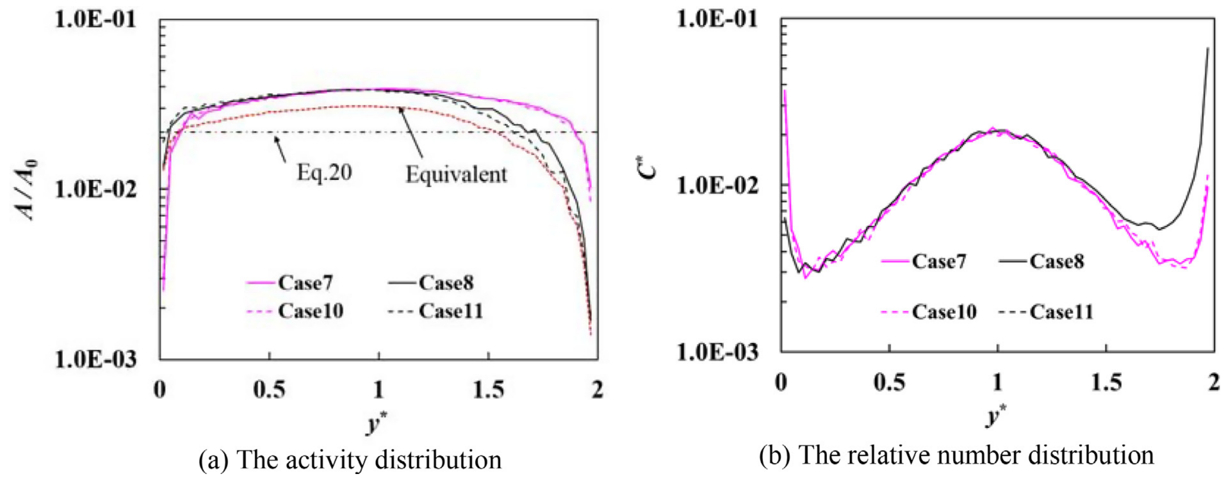

Fig. 13. The distribution of activities and relative number in the outlet along the wall-normal direction when the gravity is considered and half-lie is 7 s.

Table 2
The relative deposition number (ζ) and activity error (Δ_A) in the outlet.

Case	ζ_{south}	ζ_{north}	Δ_A	
			$T_{1/2}$ = 7 s	$T_{1/2}$ = 600 s
1	15.91%	15.89%	44.76%	−1.68%
2	15.29%	15.37%	41.81%	−2.38%
3	15.00%	14.95%	40.68%	−2.61%
4	15.83%	16.00%	44.61%	−1.60%
5	15.16%	15.17%	41.77%	−2.34%
6	15.03%	14.90%	41.13%	−2.62%
7	16.37%	15.35%	44.32%	−1.71%
8	21.09%	0.00%	24.95%	−2.71%
9	94.87%	0.00%	–	–
10	17.34%	13.94%	43.81%	−1.97%
11	22.42%	0.00%	27.46%	−1.45%
12	100.00%	0.00%	–	–

wall. If the diameter is 10 μm, almost all particles have deposited in the bottom wall before they arrive at the outlet. When the diameter is 0.1 μm, the activity error is similar with that without gravity. When the diameter is 1 μm, the activity errors are about 25% and 27% for case 8 and 11.

In order to obtain the dependence of activity error on the half-life, more radionuclides with different half-lives were employed in the simulation. The results are shown in Fig. 14 including cases 2 and 8. Because the activity errors are similar for the cases numbered 1–6, 7 and 10, the case 2 is selected to represent these cases. The horizontal ordinate of the figure is the ratio of half-life to the mean airflow time though the channel. It can be found that the activity error decreases when the half-life becomes larger. In case 2, the activity error is within ±5% if the half-life is larger than a half of the mean airflow time. But in case 8, the activity error decreases to zero when the half time is equal to about 0.3 times of airflow time, but continues to decrease to the minimal percentage of −13%. When the half-life increases, the radioactive decay slows down. But the long residence times will still result in the obvious reduction of activity for the large amount of particles migrating from the areas near the upper wall. At that time, the mean activity will be smaller than the estimate by air. When the half-life is 7.5 times larger than airflow time, the final activity error is less than 5%.

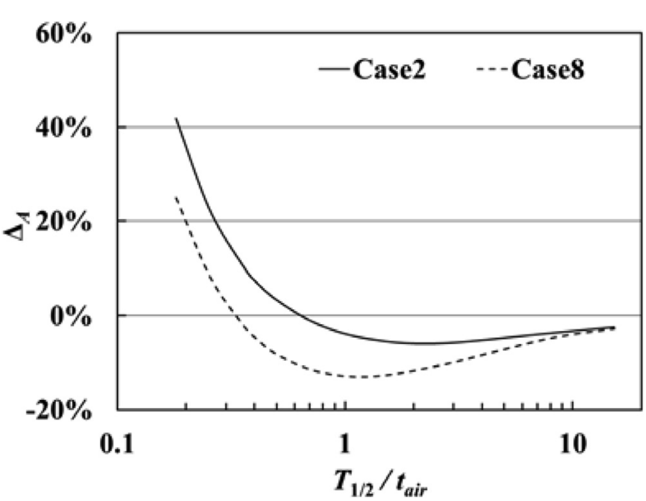

Fig. 14. The dependence of half-life on activity error for case 2 and 8.

4. Conclusion

This paper has established a Lagrangian trajectory model and used a quick numerical method to simulate radioactive aerosols transport and radioactive decay in a wall-bounded air flow in order to establish the relationship between monitored activities in channel outlet and initial activities. According to different particle diameters and densities, 12 cases have been studied in the simulation. The dimensionless deposition velocity has been validated by comparing with Wood's predictions and experienced gravitational settling velocity.

The results show that particles will not distributed uniformly in the channel and turbophoresis is an important factor on particle transport in the wall-bounded flow. Particles tend to accumulate in areas in channel center and near the wall. When gravitational settling is not considered, turbulence dominates particle transport in the main flow area. The Brownian diffusion mainly influences the deposition process in the viscous layer. When gravitational settling is considered, the 10 μm particles have almost entirely deposited in the wall within 7000 time units. Affected by the gravity, all particles in the viscous layer near the bottom wall will deposit. In the areas near the upper wall, the comparison between the gravity and Brownian diffusion leads to the settling of micron particles to the main flow and no deposition in the upper wall, but only a little reduction of the depositions for submicron particles.

Due to the effect of turbophoresis, the particles residence times in the channel will be different with the local airflow time where particle arrives. Especially, the particles migrating from the main flow field toward the wall will take shorter time than the airflow near the wall. In addition, the gravitational settling will cause particles migrating across the channel, so the residence times of particles in the upper channel are larger than the mean airflow time. The complex distribution of particle residence times will influence the activity distribution in the outlet especially for the short half-lived radionuclides.

According to the present simulation, the submicron particles will deposit by 15% on each wall, the mean activity in the outlet when half-life is 7 s will be more than 40% larger than the activity estimated by the decay calculation using the mean airflow time. However, the deposition of micron particles will increase to about 22% on the bottom wall when gravitational settling is considered. The mean activity when half-life is 7 s is larger than the estimated activity by about 25%. When the half-life becomes larger, the activity error decreases. If the final activity error is less than 5%, the half-life has to be 7.5 or 0.5 times larger than the mean airflow time for the situations when gravitational settling is considered or not, respectively. It can be seen that radioactive decay cannot be ignored or simply processed for the activity estimate when short-lived radionuclides are transported in a long distance pipe or duct.

Acknowledgements

This research is supported by National Natural Science Foundation of China (No. 11575113): Study on transport mechanism of trace radioactive aerosol in the small-scale spaces, and the key program of National Natural Science Foundation of China (No. 11535009): Research on the fission gas removal mechanism with molten salt medium at high temperature.

Appendix A. Supplementary data

Supplementary data to this article can be found online at https://doi.org/10.1016/j.anucene.2019.05.023.

References

Regulatory guide 1.45, Guidance on monitoring and responding to reactor coolant system leakage, Revision 1, U.S. Nuclear Regulatory Commission, May 2008.

International standard-Sampling airborne radioactive materials from the stacks and ducts of nuclear facilities, ISO 2889, Second edition, March 15, 2010.

Brooke, J.W., Kontomaris, K., Hanratty, T.J., McLaughlin, J.B., 1992. Turbulent deposition and trapping of aerosols at a wall. Phys. Fluids A 4 (4), 825–834.

Sardina, G., Schlatter, P., Brandt, L., Picano, F., Casciola, C.M., 2012. Wall accumulation and spatial localization in particle-laden wall flows. J. Fluid Mech. 699, 50–78. https://doi.org/10.1017/jfm.2012.65.

Lau, T.C.W., Nathan, G.J., 2014. Influence of Stokes number on the velocity and concentration distributions in particle-laden jets. J. Fluid Mech. 757, 432–457.

Narayanan, C., Lakehal, D., 2003. Mechanisms of particle deposition in a fully developed turbulent channel flow. Phys. Fluids 15 (3), 763–775.

Marchioli, C., Giusti, A., Salvetti, M.V., Soldati, A., 2003. Direct numerical simulation of particle wall transfer and deposition in upward turbulent pipe flow. Int. J. Multiph. Flow 29, 1017–1038.

Jebakumar, A.S., Premnath, K.N., Magi, V., Abraham, J., 2019. Fully-resolved direct numerical simulations of particle motion in a turbulent channel flow with the lattice-Boltzmann method. Comput. Fluids 179, 238–247.

Chiou, M.C., Chiu, C.H., Chen, H.S., 2011. Modeling particle deposition from fully developed turbulent flow. Appl. Math. Model. 35, 3238–3254.

Kim, Y., Yiacoumi, S., Nenes, A., Tsouris, C., 2017. Incorporating radioactive decay into charging and coagulation of multicomponent radioactive aerosols. J. Aerosol Sci. 114, 283–300.

Aloyan, A.E., Louzzan, P.I., Arutyunyan, V.O., 2000. Numerical modelling of regional and global transport and coagulation of radioactive aerosol from hypothetical accidental sources. J. Aerosol Sci. 31, 420–421.

Eslinger, P.W., Bowyer, T.W., Cameron, I.M., Hayes, J.C., Miley, H.S., 2015. Atmospheric plume progression as a function of time and distance from the release point for radioactive isotopes. J. Environ. Radioact. 148, 123–129.

Jiménez-Ramos, M.C., Manjón, G., Abril, J.M., 2006. Influence of sampling air flow rate in the decay correction applied to the determination of ^{7}Be and short-lived radionuclides in aerosol samples. Atmos. Environ. 40, 7215–7221.

Li, Y., Gu, W., He, J., Wang, D., 2018. A new method for simulating aerosols Brownian coagulation based on finite active samples assumption. Ann. Nucl. Energy 115, 534–541.

Gensdarmes, F., Boulaud, D., Renoux, A., 2000. Experimental study of the electrical charging of radioactive aerosols. J. Aerosol Sci. 31, S1025–S1026.

Guha, A., 2008. Transport and deposition of particles in turbulent and laminar flow. Annu. Rev. Fluid Mech. 40, 311–341.

Li, Y., Gu, W., Wang, D., 2018. Direct numerical simulation of polydisperse aerosol particles deposition in low Reynolds number turbulent flow. Ann. Nucl. Energy 121, 223–231.

Gu, W., Wang, D., Li, Y., He, J., He, Y., 2019. A stochastic method in simulating particles transport and deposition in wall-bounded turbulent flow. Ann. Nucl. Energy 127, 12–18.

Mito, Y., Hanratty, T.J., 2002. Use of modified Langevin equation to describe turbulent dispersion of fluid particles in a channel flow. Flow Turbul. Combust. 68, 1–26.

Wang, B., Zhang, H.Q., Manhart, M., Chan, C.K., 2011. A numerical study on statistical temporal scales in inertia particle dispersion. J. Comput. Appl. Math. 235, 3087–3816.

Wood, N.B., 1981. A simple method for the calculation of turbulent deposition to smooth and rough surfaces. J. Aerosol Sci. 12 (3), 275–290.